Research article

Journal of RAMAN SPECTROSCOPY

Received: 14 October 2016 Revised: 12 December 2016 Accepted: 1 January 2017 Published online in Wiley Online Library

(wileyonlinelibrary.com) DOI 10.1002/jrs.5106

# Micro-Raman spectroscopy and complementary techniques (hXRF, VP-SEM-EDS, $\mu$-FTIR and Py-GC/MS) applied to the study of beads from the Kongo Kingdom (Democratic Republic of the Congo)

Alessia Coccato,[a]* Mafalda Costa,[a,b] Anastasia Rousaki,[c] Bernard-Olivier Clist,[d] Karlis Karklins,[e] Koen Bostoen,[d] Ana Manhita,[b] Ana Cardoso,[b] Cristina Barrocas Dias,[b,f] António Candeias,[b,f] Luc Moens,[c] José Mirão[b,g] and Peter Vandenabeele[a]

**In the framework of the inter-disciplinary KongoKing project, a set of beads from archaeological excavations in the Democratic Republic of the Congo was analysed by means of a minimally invasive, multi-analytical approach based on micro-Raman spectroscopy. The full characterization of the materials, including glassy network, opacifiers and colorizers, was achieved thanks to the combination of data from handheld X-ray fluorescence, variable pressure scanning electron microscopy coupled with energy-dispersive X-ray spectrometry, micro-Fourier transform infrared spectroscopy and pyrolysis coupled to gas chromatography and mass spectrometry. The obtained chemical information was used to fill the existing gap in the chemical study of beads from Western Central Africa. The cobalt-rich blue beads were found to be of Central European origin, while the copper-rich turquoise beads were manufactured using distinct copper sources. Cadmium yellow and cadmium red are the colourants responsible for the bright colours of bead types 10 and 12, respectively. The type 12 beads were found to be composed of glass covered with a waxy layer tentatively identified as Japan wax. Prosser-moulded bead type 9 was coloured by means of a chrome–tin pigment, while a combination of Mn and Fe is responsible for the black colour of the type 47 beads. Cuprite is most likely responsible for the red hue of glass layers from type 14. The dark palm green exterior of the type 17 bead was produced by using a combination of Cu and Fe compounds; iron was the only chromophore detected in the Indian red decoration.** 

*Additional Supporting Information may be found online in the supporting information tab for this article.*

**Keywords:** micro-Raman spectroscopy; archaeometry; Kongo Kingdom; glass beads; Japan wax

## Introduction

This work focuses on the analysis of beads excavated from sites associated to the Kongo Kingdom. The KongoKing Project (http://www.kongoking.org/) is devoted to the study of the origins and history of the Kongo Kingdom, using an inter-disciplinary approach that includes archaeology and archaeometrical research, as well as historical linguistics.[1–6]

The Kongo Kingdom is thought to have been founded in the late 13th–early 14th centuries. However, as no written accounts exist prior to the arrival of the Portuguese in 1483, this date has been

* *Correspondance to: Coccato Alessia, Department of Archaeology, Archaeometry Research Group, Ghent University, Sint-Pietersnieuwstraat 35, B-9000 Ghent, Belgium.*
*E-mail: raman@ugent.be*

a *Department of Archaeology, Archaeometry Research Group, Ghent University, Sint-Pietersnieuwstraat 35, B-9000, Ghent, Belgium*

b *HERCULES Laboratory, University of Évora, Palácio do Vimioso, Largo Marquês de Marialva 8, 7000-554, Évora, Portugal*

c *Department of Analytical Chemistry, Raman Spectroscopy Research Group, Ghent University, S-12, Krijgslaan 281, B-9000, Ghent, Belgium*

d *Department of Languages and Cultures, BantUGent – UGent Centre for Bantu Studies, Ghent University, Blandijnberg 2, 9000, Ghent, Belgium*

e *Material Culture Research, Parks Canada Ottawa, Ontario, Canada*

f *Department of Chemistry, School of Science and Technology, University of Évora, Colégio Luís António Verney, R. Romão Ramalho, 59, 7000-671, Évora, Portugal*

g *Department of Geosciences, School of Science and Technology, University of Évora, Colégio Luís António Verney, R. Romão Ramalho, 59, 7000-671, Évora, Portugal*

estimated on the basis of the king's genealogy records, which can be found in written accounts from the 16th and 17th centuries.[3],[7] Contact with Europe and Europeans made a huge impact on the kingdom's society. Christianity was widespread thanks to its introduction by European missionaries, and European goods, such as glass beads, were part of the trade activities developed between Europe and the Kongo Kingdom.[1–3],[8],[9]

In African societies, glass beads were used to make jewellery pieces and amulets and also marked the hierarchical position of the person who wore them. Many glass studies have focused on beads, of European origin, found in Africa and North America.[6][10–12] Traditionally, glass bead studies were based solely on typology,[13–15] but the focal point of these studies has progressively shifted towards the chemical characterization of glass.[6],[10],[12][16–22]

The current article focuses on the glass beads recovered between 2013 and 2015 from eight sites along the Inkisi River valley and one on the southern part of the Bangu range, in the Democratic Republic of the Congo (DRC). This area was once home to the capitals of three of the major provinces: Mbata, Mpangu and Nsundi. These provinces, while not as important as the capital – Mbanza Kongo – were important symbolic, administrative and economical centres of the kingdom.[1],[2] The beads consist of surface finds, found in the sites Marché Kengi, Voka di Kinkombo, Voka di Makela and Mbilu, and of finds from excavations held in the sites of Kindoki, Kingondo, Kinkinzi, Mbanza, Mbilu and Ngongo Mbata (the location of the sites can be found in Fig. S1). The dating of the surface finds was based on the manufacturing period of the artefacts. In Kinkinzi, Mbanza and Mbilu, the beads were mostly found in the upper 20 cm of the excavation trenches, often associated with the 19th century pottery and clay smoking pipes. However, in Kindoki, Kingondo and Ngongo Mbata, some of the beads were found in deeper layers; the beads from Kingondo were dated to the second half of the 19th century on the basis of the associated pottery and clay smoking pipes, as well as oral history, while the ones found in Kindoki are dated to the 19th–20th centuries (trench 105) and 17th – 18th centuries (trench 100). Several beads found in Ngongo Mbata were dated to the 17th century (e.g. type 17 star bead from trench 35, dated between 1620 and 1700).

The beads in this study can be divided according to their manufacturing technique into drawn, wound or Prosser-moulded beads. Drawn beads are made from glass tubes that are chopped into segments that may be heat rounded to obtain the desired shapes; on the other hand, wound beads are manufactured by winding molten glass around a rotating metal mandrel.[12],[23] The Prosser-moulded beads, on the other hand, were manufactured using the Prosser-mould technique. This technique was first developed and patented in Great Britain, in 1840, with the single aim of making buttons. However, it was later applied, first in France, in 1862, to produce what is also known as the Bapterosses beads, and later in Bohemia. The Prosser-moulded beads were produced by mixing crushed feldspar, calcium fluoride, silica sand and metallic oxides. The next steps of the manufacture process are not entirely known, but it is thought that the mixture, bound together with milk, was pressed in gang moulds to form the desired bead form. The mould was then emptied onto a metal sheet that was placed in a kiln or oven. Afterwards, the beads could be glazed before being fired once again, making the final product a highly vitrified ceramic bead.[15],[24]

The main aim of this study is to fully characterize each glass bead type from a chemical point of view, using a minimally invasive, multi-analytical methodology. The combination of micro-Raman spectroscopy (MRS) and handheld X-ray fluorescence (hXRF) to non-destructively study beads from the Lower Congo Province was first established by Rousaki *et al.*[6] The use of MRS allows the material characterization of the glass, in terms of matrix (formers, stabilizers, flux, etc.) and colour/opacity, which, in combination with the elemental information provided by hXRF, gives insights into the glass-making technology used to manufacture the beads. Here, the data extracted from the hXRF analysis of the blue beads from the Kingondo, Kiyenga and Ngombi sites were compared with the data of the blue beads found in Kindoki,[6] on the basis of principal component analysis (PCA). Furthermore, different analytical techniques, such as variable pressure scanning electron microscopy coupled with energy-dispersive X-ray spectrometry (VP-SEM-EDS), micro-Fourier transform infrared spectroscopy ($\mu$-FTIR) and pyrolysis coupled to gas chromatography and mass spectrometry (Py-GC/MS), were implemented to the methodology proposed by Rousaki *et al.*[6] in order to give spatially resolved elemental composition and to better characterize non-glass beads.

## Materials and methods

### Materials

One hundred and forty-six beads were analysed in this study. These beads are mostly composed of glass, but three different manufacturing techniques were used to produce them. Sample description, including type, date, origin, manufacturing process, colour, length, width, number of samples analysed and total number of samples, as well as a representative picture of each bead type, can be found in Table S1. However, it is important to note that the colours observed are white, dark blue, turquoise, green, red, yellow, pink, brown and black, under the form of individually, monochrome beads, or combined in polychrome beads. The beads were measured untreated as no further cleaning or polishing was allowed by the archaeological team.

### Analytical methods

#### *Micro-Raman spectroscopy*

Raman spectra were obtained with a Bruker Optics Senterra dispersive Raman spectrometer coupled with a microscope. Point measurements were performed using a red diode laser (785 nm) and a green Nd : YAG laser (532 nm). The power is adjusted by neutral density filters: The green laser power was set to 5–12 mW, and the red one to 6–26 mW. Spectra were obtained in the range of 80–2642 and 60–2750 $cm^{-1}$ for the 785- and 532-nm lasers, respectively, allowing the recording of both the Raman spectrum of glass and of other phases of glass, opacifiers, colouring agents, etc. The system uses a thermoelectrically cooled CCD detector, operating at −65 °C. Laser power, total measuring time and number of accumulations were set to obtain good-quality Raman spectra (good signal-to-noise ratios). The instrument is controlled by Bruker OPUS software. The collected Raman spectra were processed in GRAMS (Thermo Fisher Scientific). To cover possible sample inhomogeneity, for each bead sample, we recorded at least three different spectra for the identification of both glass and other mineral phases.

All the spectra of the glass matrix here reported were excited with the green (532 nm) laser. For the crystalline phases, we rely on both lasers for identification. The segment baseline correction was performed in GRAMS according to published literature.[25–28] The same software was used to deconvolute the glass massifs in

its silicatic units components.[6],[27],[29–31] The $Q^n$ symbols are used to indicate such units, as in Rousaki *et al.*[6] The peak fitting procedure allowed the identification of specific silicate unit vibrations, and the performance of some qualitative considerations based on the spectral features such as the positions of maxima of the bending and stretching massifs ($x\ \nu_{max}$ and $x\ \delta_{max}$ respectively), the polymerization index $I_p$ (area ratio bending massif to stretching massif), etc.[6],[25–28],[32–34]

*Handheld X-ray fluorescence*

The elemental analysis was performed with a commercial hXRF instrument (Olympus InnovX Delta). The measurements were conducted in air, inside a shielded chamber, with a live time of 300 s. A tube voltage of 40 kV and a current of 100 μA was applied to the rhodium (Rh)-based X-ray source, delivering a $3 \times 3$ mm$^2$ collimated or $5 \times 5$ mm$^2$ uncollimated polychromatic X-ray beam for excitation. The emerging X-ray fluorescence is detected using a silicon drift detector (SDD). The instrument was connected to a portable computer that controls and monitors the actual XRF measurements. In order to avoid the effect of sample shape and dimensions, multiple spectra were recorded for each bead. The spectra were treated with the 'analysis of X-ray spectra by iterative least squares' (AXIL) and MICROXRF2 software tools.[35],[36] The contribution from the shielded chamber was measured and concluded to be insignificant on the outcome. This kind of analysis provides qualitative information,[37],[38] in order to identify groups of similarities[37] and the elemental composition of the measured beads.

A blue set of beads, from Kindoki burial sites, published in a previous work,[6] were compared with the blue beads from the current study. The aim was to find clusters of similarities or to differentiate beads with the same colour among different sites and thus possibly conclude on their origin. The Kindoki types 11, 22 (former type 1) and 23 (former type 4) dark blue beads were measured again in order to avoid interferences on the data caused by the different characteristics of the hXRF instruments used in this study and in a previous study.[6]

After the data treatment by AXIL, the results were gathered in an Excel sheet and normalized using the Si counts. Elemental bi-plots were generated in order to have a better understanding of the data collected. The results were also imported into the SPSS STATISTICS 22 (IBM) software for further data treatment. The use of PCA and the protocol used for pre-data treatment will be briefly discussed here. After the aforementioned spectra fitting, all the measurements were averaged over types, and possible sub-typologies. Elements such as Ar and Rh (K and L lines) were excluded as they do not contribute to the analysis along with Cr, Zr and U. After normalization by Si and scaling the data by the square root, outlier labelling via SPSS was applied [a value of $g = 2.2$ was used for the calculation of the upper and lower limits (quartiles) of the distribution]. K, Mn and Rb were excluded and also some measurements that were recognized as outliers. By checking correlation of variables, Ti was excluded as it was correlated with Fe. Normal distribution of the elements was cross-checked with Q–Q plots, P–P plots, histograms and boxplots. From the remaining elements, Ca, Fe, Cu, Zn, As and Pb were approximately normally distributed. Co, Ni and Sr were excluded as they did not meet the normality test. Moreover, Ca was excluded as it can occur as a stabilizer or in compounds that act as opacifying agents. PCA was performed, taking into account the following elements: Fe, Cu, Zn, As (K lines) and Pb (L lines). By observing the scree plots, three factors were extracted. The PCA was performed with oblique matrix rotation, and the Kaiser–Meyer–Olkin measure of sampling adequacy criteria was measured in order to check if the factor analysis was acceptable in the first place.

*Variable pressure scanning electron microscopy coupled with energy-dispersive X-ray spectrometry*

The VP-SEM-EDS analyses were carried out using a Hitachi™ S3700N SEM coupled to a Bruker™ XFlash 5010 SDD EDS Detector®. The samples were analysed at an accelerating voltage of 20 kV and at low vacuum (40 Pa). The images were acquired in the backscattered mode.

This analytical technique was used to give a more detailed insight into the elemental composition of the polychrome, multi-layered, by means of elemental mapping, and to perform point analysis on the monochrome beads.

*Micro-Fourier transform infrared spectroscopy*

Infrared analysis was performed on the type 12 red bead found in Mbanza. A small sample of the bead was analysed in transmission mode after being compressed in an EX'Press micro-compression diamond cell (1.6 mm, STJ-0169). For each spectrum, 64 scans were recorded with a spectral resolution of 4 cm$^{-1}$ using a Bruker Tensor 27 spectrometer coupled to a Hyperion 3000 microscope, equipped with a mercury–cadmium–telluride detector (working range, 4000–600 cm$^{-1}$). The instrument is controlled by the Bruker™ OPUS© 7.2 software.

*Pyrolysis coupled to gas chromatography and mass spectrometry*

A micro-sample of approximately 500 μg was collected from the type 12 red bead found in Mbanza and selected for analysis with Py-GC/MS. A system with a Frontier Lab PY-3030D double-shot pyrolyzer was used. The interface was maintained at a temperature of 280 °C. The pyrolyzer was coupled to a Shimadzu GC2010 gas chromatographer, also coupled to a Shimadzu GCMS-QP2010 Plus mass spectrometer. A capillary column Phenomenex Zebron-ZB-5HT (30-m length, 0.25-mm internal diameter, 0.50-μm film thickness) was used for separation, with helium as carrier gas, adjusted to a flow rate of 1.5 ml min$^{-1}$. The splitless injector operated at a temperature of 250 °C. GC temperature programme was as follows: 40 °C during 5 min, ramp until 300 °C at 5 °C min$^{-1}$ and then an isothermal period of 3 min. Source temperature was placed at 240 °C, and the interface temperature was maintained at 280 °C. The mass spectrometer was programmed to acquire data between 40 and 850 m/z. The sample, previously derivatized with 3 μl of tetramethylammonium hydroxide (25% in methanol) in a 50-μl Eco-cup capsule, was placed in the double-shot pyrolyzer using an Eco-stick. The capsule was placed in the pyrolysis interface, followed by a 2-min helium purge. The sample was pyrolyzed using a single-shot method at 500 °C during 12 s. Compound identification was performed using AMDIS software integrated with NIST-Wiley database.

## Results and discussion

In this section, we will present the results on the studied beads. First, the overall composition of the beads will be discussed (i.e. the glass, based on MRS results – baseline-corrected Raman spectra[25–28]), starting with the monochrome beads, and then moving on to the more complex polychrome ones. Afterwards, the crystalline phases, opacifiers and colouring agents will be presented for the monochrome and polychrome beads, which

complete the characterization of the beads by using the proposed multi-analytical approach.

## Glass

### *Monochrome beads*

*Blue (types 5 and 6).* The Raman spectra of the blue beads of types 5 and 6 (Table S1) show evident similarities regarding their glass signature [Fig. 1, spectra a (type 5), b and c (type 6)]. In general, the glass type is recognized as mixed alkali, on the basis of the position of the $x\ \nu_{max}$ (1085–1100 $cm^{-1}$). The calculated polymerization index $I_p$ is of approximately 1.1 for type 5 and 0.8 for type 6, suggesting firing temperatures of *ca* 1100 and 1000 °C, respectively.[25]

An intense band sometimes appears at *ca* 990 $cm^{-1}$ (Fig. 1, spectrum b). It is attributed in literature to $\nu\ Q^2$ vibrations.[26],[34] $Q^2$ units are those related to the presence of divalent stabilizers, and other ions including Pb and Cu, or Co.[26],[27],[32] The attribution to a Co-containing silicate, which might be responsible for the blue colour, is supported by hXRF results, and literature.[32] However, Cu and Pb were also detected by hXRF, which could suggest the incorporation of these elements into a relatively organized structure in alkali silicate glasses, whose Raman active mode corresponds to what was observed.[26] The lead content, on the basis of the Raman spectra of glass, appears to be low, as suggested by the $\nu\ Q^2$ contribution to the total stretching massif area, and the position of the stretching maximum $x\ \nu_{max.}$[27]

*Turquoise (pendant and type 48).* Again, the two studied turquoise samples [Table S1, Fig. 1, spectra d (pendant) and e (type 48)] belong to the family of mixed alkali glasses, showing $x\ \nu_{max}$ values of 1092–1096 $cm^{-1}$, and $I_p$ around 1 (corresponding firing temperature of *ca* 1100 °C).[25] As many crystalline phases overlap with the glass signature, no additional information on the glass matrix could be obtained.

*Pink (type 9) and yellow (type 10).* Although the colour of these beads is different, their morphology is similar, therefore suggesting a common manufacturing technique (Table S1). MRS of both bead types yielded spectra attributable to glassy materials, but not strictly to glass [Fig. 1, spectra f (type 9) and g (type 10)]. In fact, the stretching and bending massifs of silicate units are visible, giving an $I_p$ of *ca* 2.5. This value is anomalous and extremely high compared with that of the other studied glasses, signifying a highly polymerized silicate structure.[34] Similar spectra, showing predominant $\delta$ Si–O, are reported in literature for stonewares, porcelain and porcelain glazes.[34] These results are congruous with the identification of these beads as Prosser moulded, i.e. highly vitrified ceramic beads.[15],[24]

*Red (type 12).* The inability to determine the characteristic glass Raman bands in the type 12 beads (Table S1) led to the use of different analytical techniques in an attempt to uncover the composition of these beads. Micro-FTIR revealed that a mix of kaolinite (bands at 3694, 3618, 1038, 914, 790 and 698 $cm^{-1}$) and wax material (bands at 2955, 2920, 2851, 1738, 1631, 1464, 1380, 1321 and 720 $cm^{-1}$), with vestigial traces of protein (bands at 1543 and 1438 $cm^{-1}$), made up the outer layer of these beads (Fig. 2). The presence of a waxy outer layer, most likely composed of Japan wax, was further confirmed by Py-GC/MS (Table S2 and Fig. S2).

Natural waxes are highly heterogeneous materials, which are solid at room temperature and highly hydrophobic. Waxes can be of animal, vegetable or fossil origin, and, chemically, most of these wax materials are made of esters of long-chain carboxylic acids and alcohols (absent in the fossil waxes) and *n*-alkanes. Japan wax, originating from the protective coatings of the kernels of the berries of some sumac plants (*Toxicodendron*, former *Rhus*, genus), growing in China and Japan, is often used as a coating material and has a peculiar composition. Japan wax does not contain wax esters, being mainly composed of triacylglycerols, with tripalmitin being the

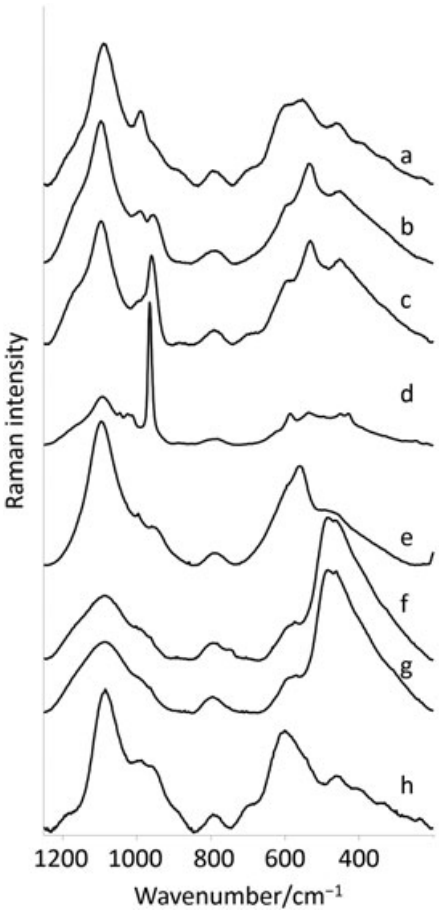


**Figure 1.** Raman spectra (baseline corrected) of the glass for the monochrome beads. (a) Type 5; (b and c) type 6; (d) pendant; (e) type 48 bead; (f) type 9; (g) type 10; (h) type 47.

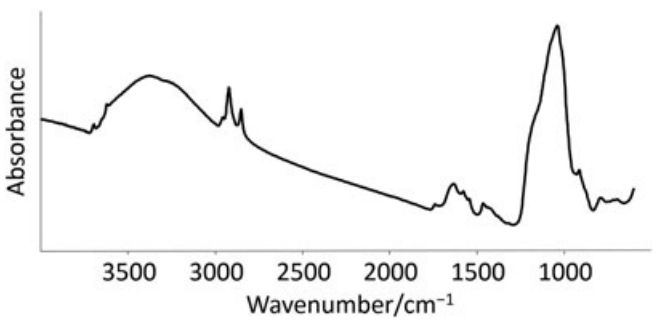


**Figure 2.** Micro-FTIR spectrum of the type 12 red bead found in Mbanza (DRC). The absorption band's assignment can be found in the text. The band at 1578 $cm^{-1}$ is thought to be connected to the colouring agent.

Journal of RAMAN SPECTROSCOPY

most abundant, and is classified as a wax due to its physical properties similar to those of beeswax.[39],[40]

The plant and animal wax materials, composed mainly with wax esters and alkanes, yield pyrograms with larger amounts of long-chain (C > 20) fatty acids and alcohols and *n*-alkanes compared with those yielded by our sample. What is present in large amounts in the type 12 bead pyrogram are even-numbered saturated fatty acids, from C14 to C18, the respective mono-unsaturated compounds (C14:1, C16:1 and C18:1), and also several dioic acids (di-C4 to di-C9). Dioic acids are frequent in samples that have large amounts of unsaturated fatty acids that tend to oxidize with time. In fact, various alteration processes occur with the ageing of wax materials, including hydrolysis of esters and TAGs, migration and crystallization of *n*-alkanes and fatty acids, sublimation of *n*-alkanes and also oxidation and polymerization, which may occur depending on the preservation state of the material.[41] Moreover, the analytical methodology applied can also account for some changes of the original material: Pyrolysis, for instance, will contribute to the hydrolysis of any ester present in the original sample.[41]

Type 12 bead's pyrogram also shows several compounds that could arise from the pyrolysis of proteins. These are minor compounds and might arise from microbial contamination or due to the extensive handling of the bead. Squalene and cholesterol derivatives are also present in the samples, which are also likely to arise from sample handling without gloves. It is unknown if small amounts of other wax material and/or plant fat were added to the Japan wax, which could account for the alkanes, alcohols, long-chain fatty acids and diacids present in the pyrogram.

On the other hand, the $\mu$-FTIR spectra of the interior part of the bead showed bands that could be attributed to aluminosilicates. Likewise, the VP-SEM-EDS analysis confirmed that the interior part of the bead is composed of a Na-rich glass, suggesting that the absence of the characteristic glass Raman bands was caused by the strong luminescence attributed to the presence of a Japan wax outer layer.

*Black (type 47).* The black type 47 (Table S1) bead's glass signature is shown in Fig. 1, spectrum h. It is, again, of the mixed alkali family, possibly including some lead, as suggested by the relatively low $x\ \nu_{max}$ position (1084 $cm^{-1}$),[27] by a calculated $I_p$ of 0.7 corresponding to *ca* 1000 °C firing temperature,[25] and by the relative contribution of $\nu\ Q^3$ to the overall stretching massif.[25],[27] The obtained information suggests a similarity with the black bead of former type 16 published by Rousaki *et al.*,[6] currently labelled as type 18.

*Polychrome beads*

*Types 14 and 49.* The type 49 bead is composed of a complex multi-layered structure (Table S1), where an inner core of light glass (opaque bluish white, with an intermediate translucent bluish layer) is covered by a thick red layer with a transparent intermediate layer. Finally, a bluish white opaque layer and a transparent blue one are present. The MRS glass spectra were collected on the red, transparent blue and bluish white glasses. The two shades of blue appear similar to each other as regards the glass composition, having similar values for the stretching and bending maxima [1094 and *ca* 585 $cm^{-1}$, Fig. 3, spectra a (whitish) and b (bluish)], and the calculated $I_p$ (0.8), indicating firing temperature of *ca* 1000 °C. From the spectral information, some lead is expected to be present in the glass matrix, as well as other cations.[27] On the other hand, the red glass appears different (Fig. 2, spectrum c), as regards its bending maximum (*ca* 540 $cm^{-1}$), and the absence of a clear indication of the presence of lead ($x\ \nu_{max}$ 1096 $cm^{-1}$). Also, its $I_p$ is slightly higher than for the other glasses (0.9), but still indicating the same range of firing temperatures. The band at *ca* 990 $cm^{-1}$, present in the blue and bluish white and absent in the red, is likely to be related to the presence of Co, or Cu, in the silicatic glassy network.[26],[27],[32] These chromophore ions are not expected to be present in the red glass.

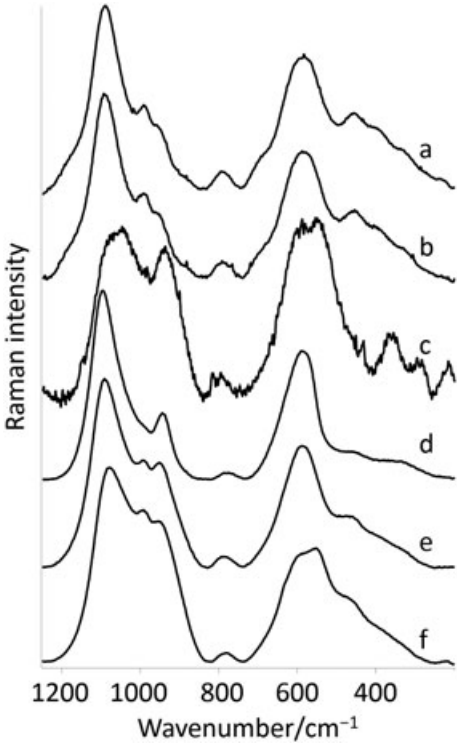


**Figure 3.** Raman spectra (baseline corrected) of the glass for the polychrome beads. (a and b) Glass signature of the two blue hues found in the type 49 bead; (c) glass signature of the red glass from the type 49 bead; (d) blue glass found in the type 14 bead; (e) glass signature of the green glass from the type 17 bead; (f) glass signature of the brown decorations of the type 17 bead.

The cylindrical multi-layered type 14 bead (Table S1) presenting blue, white and red colours was analysed as well, but the signature of the glass could only be successfully recorded on the blue part (Fig. 3, spectrum d). High fluorescence characterized the spectra collected from the red glass, and the presence of crystalline phases overlapping with the glass bending massif in the white area (refer to subsequent discussion) strongly hampered the characterization of the glass. From the blue glass, an $I_p$ of 0.8 was calculated. The $x\ \nu_{max}$ and $x\ \delta_{max}$ are similar to those observed for the type 49 bead blue glass, but different from the blue beads of types 5 and 6. In fact, notwithstanding the blue colour of this glass, the $Q^2$ structure at *ca* 990 $cm^{-1}$ present there, and attributed to the presence of divalent ions such as Co or Cu, is only observed in the type 49 bead.

*Type 17 (star bead).* The so-called star bead shows a variety of colours (Table S1). The different shades of green/brown glass show all the same characteristics [Fig. 3, spectra e (green) and f (dark decoration)]. The green glass of the star bead shows the lowest maxima of $x\ \nu_{max}$ (1080 $cm^{-1}$) and the lowest calculated $I_p$ (0.5).[25] This information, together with the ratio of the 990 $cm^{-1}$ band to the total

of the stretching massif,[27] suggests the presence of lead in the glass matrix. Moreover, as from hXRF analysis, this glass bead is enriched in Cu and Fe. Cu in glass gives a light blue colour, and a high $Fe^{2+}/Fe^{3+}$ ratio the typical bottle green hue.[42–45] The presence of divalent ions enhances the $\nu$ $Q^3$ contribution to the stretching modes,[32] promoting the appearance of the band at *ca* 995 $cm^{-1}$.

## Crystalline phases, opacifiers and colouring agents

### *Monochrome beads*

*Blue (types 5 and 6).* The blue beads from types 5 and 6 (Table S1) were found to have different hues, which include dark navy blue, ultramarine, royal blue and medium blue. Based purely on visual observation, these beads were divided into subgroups according to both colour and morphological characteristics, such as the presence of a lighter inner core or the presence of vertical lines parallel to the polyhedron's edges. However, chemical analysis showed no significant changes in composition that could justify this subdivision, as indicated by the results of PCA. In fact, PCA was not able to underline definite trends between the subgroups, even when compared against the blue beads from the Kindoki burial sites, published in previous work by Rousaki *et al*.[6] In general, Kindoki type 22 (former type 1), Kindoki type 23 (former type 4), and types 5 and 6 seem to contribute to a bigger group with variances being credited to type and minor hue differences (Fig. 4). Kindoki types 22 and 23 are thought to have been manufactured in Bavaria, while types 5 and 6 were most likely produced in Bohemia. These results, therefore, point towards a common Central European origin but do not allow a clear differentiation between Bavaria and Bohemia, suggesting that geographical proximity led to the use of similar recipes, and raw materials, in the manufacture of these glass beads.

Kindoki type 11, on the other hand, corresponds to a different glass bead composition, which is consistent with the hypothesis of these beads being produced in Venice.[6]

The main characteristic of the blue beads from types 5 and 6 is the presence of significant amounts of Co in their composition, detected by hXRF. This metal, which is responsible for their dark blue colour,[42] is generally accompanied by minor amounts of copper, which was added either unintentionally, as an impurity in the cobalt source,[46] or intentionally to produce lighter hues. On the other hand, manganese, which was detected in several beads, was most likely added to produce darker and more purplish hues.[42] In addition to copper, variable amounts of Ni, Pb, Zn, As and Bi were found to be associated with cobalt. Cobalt, while not a rare metal, is generally exploited as a by-product of copper, nickel, lead and zinc extraction.[46] Likewise, cobalt arsenates or arsenosulfides are also quite commonly found in exploitable deposits.[46] The parageneses of Co-bearing and Bi–Cu–Pb minerals, although rarer, can be found, for example, in massive or stratabound sulfide deposits.[47] Thus, the slight differences in composition found in the hXRF results can easily be explained by the natural variability in the Co raw material source.

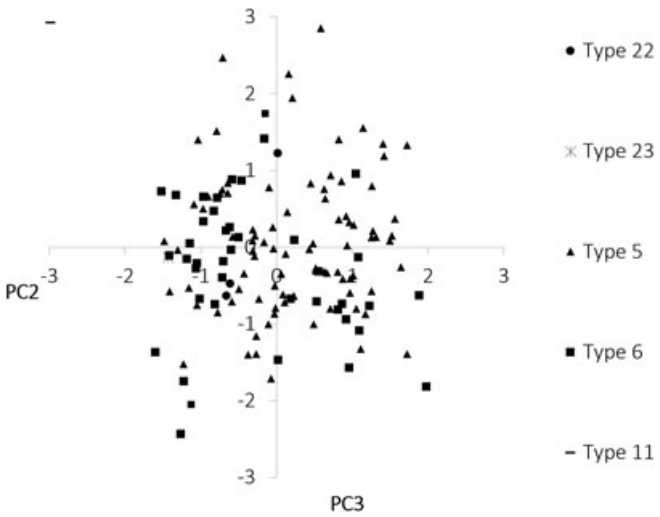


**Figure 4.** Score plot for PC2 and PC3. Different symbols represent different blue bead types. Types 11, 22 and 23 were previously studied in Rousaki *et al*.[6]

MRS revealed the presence of quartz due to the characteristic bands at approximately 204, 356 and 401 $cm^{-1}$.[48] Bands at 143, 396, 516 and 637 $cm^{-1}$ were attributed to anatase,[48],[49] although in general only the first was observed. The band at 151 $cm^{-1}$ can also be attributed to anatase[50] or brookite.[48] Titanium dioxide can usually be found in one of the three most common crystalline phases: anatase, rutile and brookite. Raman spectroscopy has long been used to identify and distinguish anatase from rutile,[51] but recent studies have shown that the vibration mode associated to the $A_{1g}$ active mode of the anatase structure can be found from 142 to 159 $cm^{-1}$ depending on the temperature of formation of this mineral,[49],[50] making the identification of the correct titanium dioxide when only the 142–159 $cm^{-1}$ band is present, and especially in combination with the silicate bending massif, extremely difficult.

The relatively high amount of Ca, detected by hXRF, in conjunction with the bands at 450–453, 956–960 and approximately 1000 $cm^{-1}$, attributed to $\nu_2$ $PO_4^{3-}$, $\nu_1$ $PO_4^{3-}$ and $\nu_1$ $HPO_4^{2-}$,[52] respectively, suggests that calcium phosphate was used as an opacifying agent.[6] Finally, the combined bands at 139–144 and 184 $cm^{-1}$ can be attributed to lead sulfates and oxysulfates,[53] although the absence of the characteristic $\nu_1$ vibration of $SO_4^{2-}$ at 957–977 $cm^{-1}$ should be noted.

*Turquoise (pendant and type 48).* The type 48 and pendant beads (Table S1) were found in different archaeological contexts but share in common their turquoise colour.

hXRF analysis of the type 48 bead revealed that Cu was used as a colouring agent. This is in agreement with the results from MRS as the sharp band found at 995 $cm^{-1}$ can be attributed to the $\nu_1$ $PO_4^{3-}$ of copper phosphates.[54] The absence of other Raman bands does not allow a clear determination of the exact copper phosphate.

Relatively small amounts of Co were also detected by hXRF. This metal could have been added in order to produce slightly darker hues, or fortuitously, as Co is a known impurity in copper ores.[46] However, a careful examination of the hXRF results also showed an enrichment in both As and Bi. The presence of an arsenic-rich compound was corroborated by MRS: The bands at 215 and 275 $cm^{-1}$ (Fig. 5, spectrum a) were attributed to arsenopyrite (FeAsS).[55] On the other hand, the presence of Bi gives important information regarding the colourant source. Bismuth is a post-transition metal that commonly occurs in lead, copper and silver ores.[56] However, it is also known to be present in skarn-type ores, rich in arsenopyrite and chalcopyrite, and with minor amounts of Co-rich minerals.[57] Thus, the association between As and Bi, which

Journal of RAMAN SPECTROSCOPY

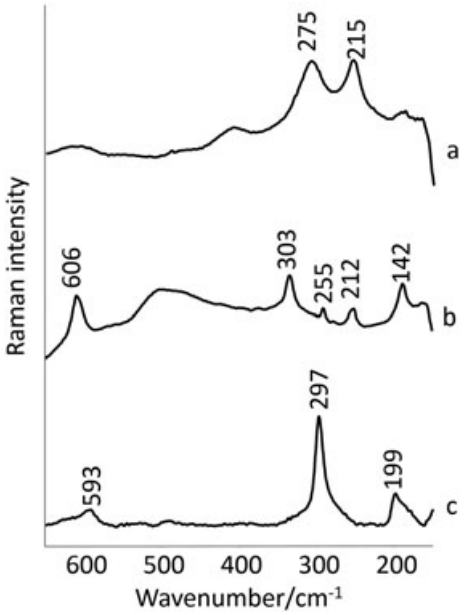


**Figure 5.** Raman spectra (baseline corrected) showing the different opacifiers and colourants found in the monochrome beads. (a) Arsenopyrite was identified in the type 48 bead; (b) cadmium sulfide and anatase were identified in the type 10 beads; (c) cadmium sulfoselenide was identified in the type 12 beads.

can be seen in Fig. 6a, suggests that the Cu-rich colouring agent used to obtain the turquoise hue characteristic of the type 48 bead came from a skarn-type ore.

Finally, the Raman band at 959 $cm^{-1}$ was attributed to $\nu_1$ $PO_4^{3-}$,[52] which, in combination with the relatively high amount of Ca, detected by hXRF, suggests that calcium phosphate was used as an opacifying agent.

MRS performed on the pendant, in conjunction with the relatively high amount of Ca, detected by hXRF, also revealed the presence of calcium phosphate: Bands at 428, 964, 1024 and 1046 $cm^{-1}$ were attributed to $\nu_2$ $PO_4^{3-}$, $\nu_1$ $PO_4^{3-}$, $\nu_3$ $PO_4^{3-}$ and $\nu_3$ $PO_4^{3-}$,[52] respectively. This mineral was most likely used as an opacifier.

As in the case of the type 48 bead, copper was found to be the main colourant, while Co was added either to obtain a darker hue or unintentionally. MRS (785-nm excitation) revealed the existence of sulfate tetrahedral oxyanions, due to the characteristic $\nu_1$ vibration at 981 $cm^{-1}$.[48],[58] According to Frost *et al.*,[58] this band can be found in the Raman spectra of complex copper(II) sulfate minerals. hXRF analysis also revealed that the pendant is enriched in Pb and Bi. The association between Cu and Pb and Bi, which can be seen in Fig. 6b and c, suggests that both Pb and Bi were present in the copper source. While the exact type of copper deposit remains, in this case, unknown, it is clear that the copper sources used to produce the type 48 and the pendant beads are different.

*Pink (type 9).* The type 9 beads found in Mbanza were identified as Prosser-moulded beads, being, therefore, chronologically assigned to the 19th century, post 1862 (Table S1).

MRS revealed the presence of quartz (465 $cm^{-1}$),[48] as well as titanium dioxide (151 $cm^{-1}$).[48],[50] Bands at 573 and 965 $cm^{-1}$ were attributed to $\nu_4$ $PO_4^{3-}$ and $\nu_1$ $PO_4^{3-}$,[52] respectively, which, in combination with the relatively high amount of Ca, detected by hXRF, suggests that calcium phosphate was used as an opacifying agent. No colouring agent was detected by MRS, but a careful analysis of the hXRF results showed an enrichment in both Sn and Cr (Fig. 6d). Chrome–tin pigments were first developed in the 1820s[59] and have since then been widely used in ceramic production to obtain hues from pink to purple and red to brown.[60–66] In order to obtain this pigment, a calcium tin silicate ($CaSnSiO_5$), also known as tin sphene, is doped with Cr(III) ions – the sphene is the host lattice, while the chromium acts as a chromophore.[60–63],[65],[66] The hue obtained depends on the Cr/Sn ratio.[61] VP-SEM-EDS analyses did, in fact, reveal the presence of particles simultaneously enriched in both Sn and Ca dispersed within the glass matrix. The fact that Cr

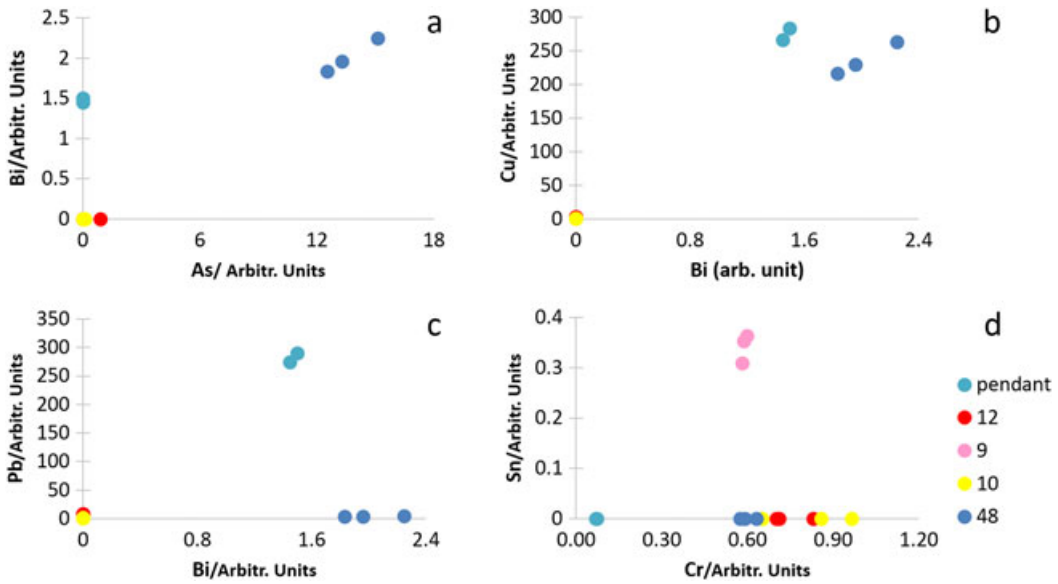


**Figure 6.** (a) Bi–As plots showing the association between these two elements in the type 48 bead; (b) Cu–Bi plot; (c) Pb–Bi plot; (d) Sn–Cr plot showing the association between these two elements in the type 9 beads. Plots (c) and (d) show a clear association between Cu, Pb and Bi in the pendant. [Colour figure can be viewed at wileyonlinelibrary.com]

was not detected can be explained by the instrument's detection limits and the minor amounts of chromium that are needed to produce the pink colour. It is important to note that the colouring agent's time frame usage and application is consistent with the identification of the type 9 beads as Prosser-moulded beads, i.e. highly vitrified ceramic beads.

*Yellow (type 10).* The yellow type 10 beads found in Mbanza were identified as Prosser-moulded beads, manufactured post-1862 (Table S1).

MRS revealed the presence of titanium dioxide[49]–[50] and quartz[48] due to the characteristic bands at 142 and 464 $cm^{-1}$, respectively. The band at 591 $cm^{-1}$, attributed to $v_4$ $PO_4^{3-}$,[52] in combination with the relatively high amount of Ca detected by hXRF, suggests that calcium phosphate was used as an opacifier. The remaining bands were attributed to the colourant cadmium yellow (CdS) (Fig. 5, spectrum b): The band at 212 $cm^{-1}$ was attributed to off-resonance multi-photon modes,[67],[68] and the band at 255 $cm^{-1}$ is characteristic of the cadmium sulfide hexagonal structure,[47],[68],[69] while the bands at 303 and 606 $cm^{-1}$ were attributed to the LO and 2LO modes.[67],[68],[70–72] The use of cadmium yellow as the colouring agent was confirmed by hXRF, which shows that high amounts of Cd are present in these beads. The relative enrichment in Zn is also noteworthy but can be explained by the cadmium source because this element is usually extracted as a by-product of zinc refining.[73–75] In fact, Zn has been detected in cadmium yellow pigments by Rosi *et al.*,[67] and the presence of this element is known to produce primrose and light yellow shades.[61] Cadmium yellow was first commercialized in 1840, 23 years after the discovery of the metal cadmium.[67],[73],[76],[77] During the 19th and 20th centuries, this pigment was used primarily by painters who believed it to be the most stable bright yellow pigment available at the time,[73],[76] but it was also used in the ceramic industry.[61],[76] Cadmium pigments were gradually removed from the market in the 1990s owing to the raising concerns regarding their toxicity.[19],[73],[77] The use of the cadmium sulfide pigment is congruous with the manufacturing process and date of these beads.

*Red (type 12).* The main characteristic of type 12 red beads (Table S1) is the absence of the characteristic glass Raman bands. In fact, the use of MRS revealed a strong luminescence, accompanied by bands at 199, 297 and 593 $cm^{-1}$ (Fig. 5, spectrum c). These bands have been attributed to the following overtone and combination modes of the cadmium red pigment ($CdS_xSe_{1-x}$): 199 $cm^{-1}$ LO (CdSe), 297 $cm^{-1}$ LO(CdS) and 593 $cm^{-1}$ 2LO(CdS).[19],[21],[71] The use of a cadmium sulfoselenide pigment was confirmed by hXRF as these beads are enriched in both Cd and Se. The visible relative enrichment in Co can be attributed to the cadmium source. Cadmium is a relatively rare element that does not usually form minerals independently. Instead, this element is usually found in zinc ores and is, therefore, a common by-product of Zn extraction.[73–75] Likewise, Co can also be produced as a by-product of the mining of zinc ores.[46] However, the amount of Zn found in these beads cannot be explained exclusively by the Cd source. VP-SEM-EDS results revealed that Zn was also present as an oxide. ZnO was most likely added as an opacifier and to diminish the glass brightness, producing a slight matte effect.[78]

Cadmium–zinc sulfoselenide has already been identified by Bouchard *et al.*[79] and Prinsloo *et al.*[21] as the colouring agent responsible for producing red glass and red glass beads, respectively. Cadmium red was first patented in Germany in 1892, but it was only commercialized in 1910.[21],[73],[77] Following the public's concerns regarding the toxicity of cadmium in the 1990s, these pigments gradually disappeared from the market.[21],[73],[77] Therefore, the use of this colouring agent indicates that this type of bead was manufactured in the 20th century.

*Black (type 47).* The hXRF results of the type 47 black beads (Table S1) revealed significant amounts of Mn and Fe in their composition. Iron and manganese have been used to produce dark coloured or black glass since the Iron Age.[80],[81] The presence of Mn usually yields a slightly purplish hue to the glass.[42] hXRF also showed an enrichment in Pb, Sb and Ca (Fig. 7a and b). The association between Pb and Sb (Fig. 7a) and Ca and Sb (Fig. 7b) suggests that lead antimonates and calcium antimonates were used as opacifying agents.

MRS revealed the presence of titanium dioxide due to the characteristic band at 146 $cm^{-1}$. As mentioned earlier, the vibration mode associated to the $A_{1g}$ active mode of anatase can shift between 144 and 159 $cm^{-1}$ according to its formation temperature.[50] However, the band at 147 $cm^{-1}$ has also been attributed to rutile,[48] making a clear identification of the crystalline phase of $TiO_2$, in this case, impossible.

*Polychrome beads*

*Types 14 and 49.* On the surface of the transparent blue glass of the type 49 bead (Table S1), many Raman bands were identified, related to silicates such as 883 and 906 $cm^{-1}$ (orthosilicates) and 584 $cm^{-1}$ ($KAlSi_3O_8$, orthoclase). Sulfates of Ca (anhydrite, $CaSO_4$) and Na (thenardite, $Na_2SO_4$) are responsible for the bands at 1017 and 992 $cm^{-1}$, respectively.[48] A variety of carbonates were

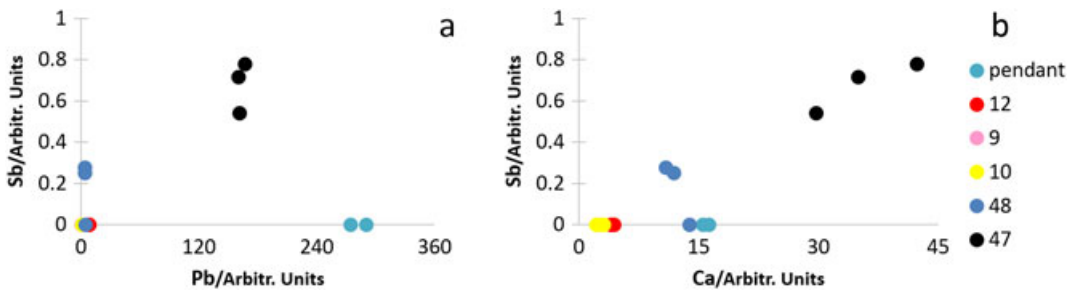


**Figure 7.** (a) Sb–Pb plot suggesting the use of lead antimonates to opacity the type 47 black bead; (b) Sb–Ca plot suggesting calcium antimonates are used as opacifying agents in the type 47 black bead. [Colour figure can be viewed at wileyonlinelibrary.com]

detected on this surface: Bands at 155 and 434 $cm^{-1}$ were attributed to malachite $Cu_2(OH)_2(CO_3)$, 284 and 1082 $cm^{-1}$ to calcite ($CaCO_3$) and the band at 1099 $cm^{-1}$ to dolomite ($CaMg(CO_3)_2$).[48] Phosphates, such as $Na_3PO_4$, are suggested by the bands at 545 and 936 $cm^{-1}$.[48] Moreover, in the whitish glass, a weak signal attributable to calcium phosphate (961 $cm^{-1}$) could be identified.[28],[48],[52] The bluish white opaque glass always showed a band at 636 $cm^{-1}$, attributed to cassiterite ($SnO_2$), a common glass opacifier.[82],[83] The spectrum of the red glass did not show any clear identification of the colourizer. Many bands attributable to silicates could be identified, at 237, 328, 415, 631 and 795–792 $cm^{-1}$.[48] Photoluminescence bands were observed, and Cr containing $Mg_2SiO_4$ could be identified (785 nm excited, 1180, 1369 and 1622 $cm^{-1}$), as well as other elements trapped in silicatic structures.[84] Such elements might give photoluminescence even when present below the detection limit or could be related to a localized inclusion. Also, here, degradation products such as bicarbonates ($NaHCO_3$) or sulfates ($MgSO_4\,H_2O$) (1047 $cm^{-1}$[48]) were identified. Moreover, the main band of a copper salt (sulfate or phosphate) is visible at 972 $cm^{-1}$.[85] The absence of other weak bands makes the identification of the exact compound impossible; however, the presence of Cu could suggest that the red glass is coloured by means of cuprite. Another copper compound, $BaCuO_2$, could be present on the basis of the bands at 640 and 585 $cm^{-1}$.[86] Unfortunately, neither Cr, nor Cu or Ba was detected by VP-SEM-EDS. This is most likely related to the fact that VP-SEM-EDS is a superficial technique, only capable of giving the elemental composition of a relatively thin surface layer.[87]

The cylindrical multi-layer bead is composed of whitish, red, whitish again and blue glass, from core to outside (Table S1). On its surface, a variety of silicate compounds relatable to the burial conditions were identified, such as micas and serpentines (bands at 179, 204, 407, 432 and 690 $cm^{-1}$[48]). The band at 968 $cm^{-1}$ can correspond to other silicates present (orthosilicates or tectosilicates – other bands at 160, 372 and 480 $cm^{-1}$), or to calcium phosphate.[48] Another phosphate salt was identified ($Na_3PO_4$), on the basis of the band at 939 $cm^{-1}$.[48] $TiO_2$ was identified as well.[50] Moreover, in the whitish glass, calcium antimonate $Ca_2Sb_2O_7$ was identified on the basis of the bands at 634 and 481 $cm^{-1}$ (Fig. 8, spectrum a), which presents a similar intensity.[25],[32],[88],[89] Elemental mapping performed by VP-SEM-EDS confirmed that the whitish glass was enriched in both Ca and Sb (Fig. 8c).

Notwithstanding the similar colour scheme of these two beads, it appears that a different opacifying technology was used, one based on cassiterite and calcium phosphate, as opposed to calcium antimonate.

*Type 17 (star bead).* The multi-layer type 17 star bead was found in Ngongo Mbata. This particular bead is a four-layered variety composed of a dark palm green exterior, opaque white, opaque Indian red and a colourless core (Table S1). The bead resembles a watermelon as it has stripes of dark palm green and whitish green. The stripes are, in fact, ridges of the corrugated second layer of opaque white glass showing though the outer semi-transparent layer.

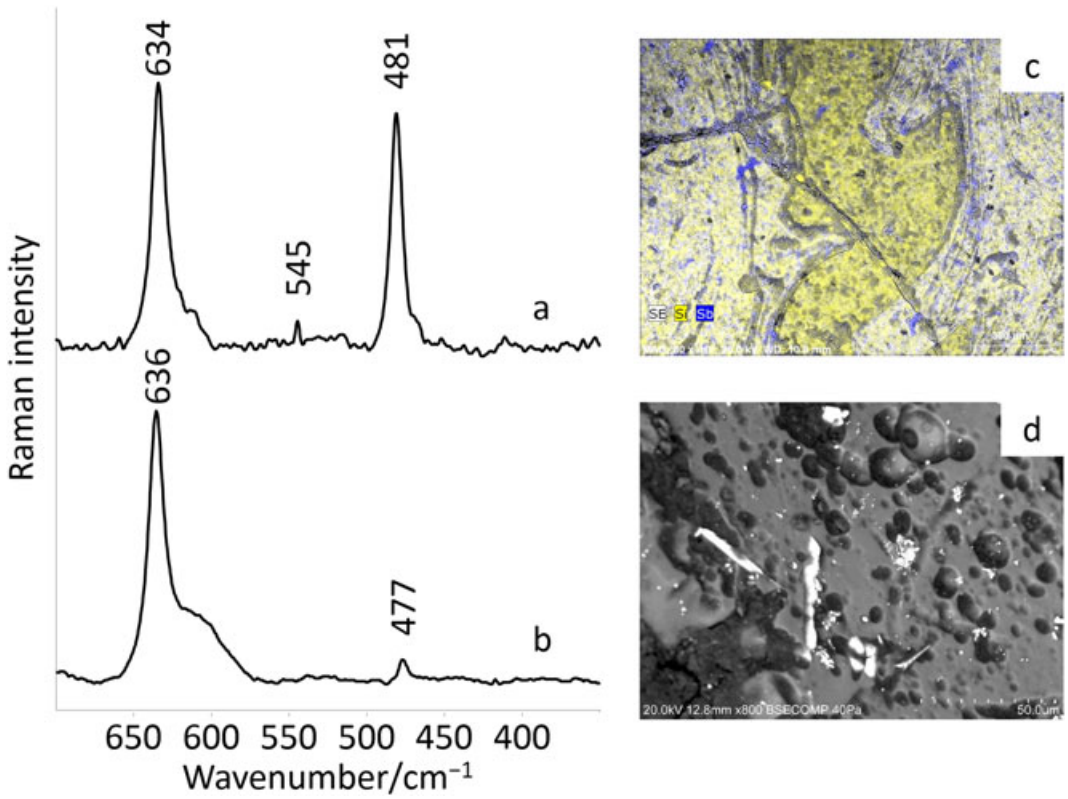


**Figure 8.** Opacifiers identified in the polychrome beads. (a) Baseline-corrected Raman spectrum of calcium antimonate identified in type 14. (b) Baseline-corrected Raman spectrum of cassiterite identified in type 17. (c) Elemental mapping of Si and Sb; areas in blue are enriched in Sb and correspond to the whitish glass surrounding the red decoration (here in yellow owing to its enrichment in Si). (d) VP-SEM image; the white areas were found to be Sn-rich particles (cassiterite) dispersed in the glass matrix. [Colour figure can be viewed at wileyonlinelibrary.com]

VP-SEM-EDS analysis did not reveal any significant changes in composition within the green layer, which led to the use of hXRF owing to its larger beam size and higher penetration. It is important to note that hXRF was only performed on the green layer and not on the opaque white and opaque Indian red decorations found in the bead's extremities. hXRF showed that both Cu and Fe were used as colouring agents. Copper ions in their divalent state can be used to produce blue glass,[42],[45] while iron can be used to produce yellow or blue hues when ferric ions or ferrous ions, respectively, are present.[42],[44],[45] The final hue produced by the presence of iron in glass is defined by the $Fe^{2+}/Fe^{3+}$ ratio, ranging from amber/brown colours to green.[42–45] This suggests that copper and iron were deliberately used to produce a darker, bluish green hue. A careful examination of the hXRF results also uncovered a significant enrichment in both Sn and Pb. MRS, on the other hand, revealed compositional differences within the green layer. A line scan with a total of 13 measurements was performed across the green external glass layer. As can be seen in Fig. S3, the aforementioned stripes are not visible under the microscope, so we cannot clearly state that these compositional differences are associated to the variable colour of the glass layer. The Raman spectra acquired were divided into four groups according to the presence or absence of crystalline phases as following: (1) group in which the bands are at 477 and 636 $cm^{-1}$, attributed to cassiterite[89] (Fig. 8, spectrum b, and Fig. 8d), as well as a band at 143 $cm^{-1}$, attributed to anatase,[49] were found; (2) group in which only bands attributed to glass were found; (3) group in which only the band at 147 $cm^{-1}$, attributed to $TiO_2$, was identified[50]; (4) group in which the 146 $cm^{-1}$ Raman band attributed to $TiO_2$,[50] was accompanied by glass bands. There was one Raman spectrum that could not be assigned to any of the groups. In this spectrum, besides the bands attributed to glass, the bands at 148, 239 and 287 $cm^{-1}$ were attributed to $TiO_2$,[50] O–Cu–OH bending modes[54] and the external lattice mode of calcite ($CaCO_3$),[90] respectively. Finally, the band at 263 $cm^{-1}$ was assigned to the transverse optical mode of covellite (CuS).[55],[91] The absence of covellite's longitudinal optical mode[55][91] can be explained by overlap with glass bands in the same region.

Regarding the outer decoration, the opaque white glass was found to be composed almost exclusively of Si by VP-SEM-EDS. The opacification of this glass layer can be explained by the presence of air bubbles, which are a known opacifying agent,[92] and is suggested owing to the characteristic morphology observed by VP-SEM-EDS. The opaque Indian red layer, on the other hand, is characterized by high concentration of Sn, found as particles dispersed within the glass matrix. Lead was also detected and is most likely contributing to the glass's opacification. The only chromophore found in this layer was iron, which has been known to produce similar brownish hues.[43],[93]

## Conclusions

The inter-disciplinary project KongoKing is the first of its kind in Western Central Africa and takes full advantage of a multi-technique chemical characterization of archaeological artefacts, such as beads. Chemical characterization of beads was already achieved for several South and Eastern African archaeological sites,[17–22] but this work only started very recently for Western Central Africa.[6] The combination of the analytical techniques proposed here proved successful in providing a full chemical characterization of European trade beads excavated in the DRC. Obtaining different types of information from MRS, hXRF, VP-SEM-EDS, $\mu$-FTIR and Py-GC/MS allowed a clarification of the origin and manufacturing techniques of the materials studied, giving new insights into the trade bead industry.

Although MRS was the technique of choice to characterize the glassy matrix in a non-destructive way, auxiliary techniques were used to complement the information obtained, enabling a better understanding of the colourizers and opacifiers used to manufacture the different bead types. In fact, MRS results show that most of the beads (with the exception of type 12) are composed of mixed alkali glass. The Raman spectra of the type 9 and 10 beads were found to be consistent with their identification as Prosser-moulded beads (highly vitrified ceramic beads). The absence of the characteristic glass Raman bands in the type 12 beads, masked by a heavy fluorescence, led to the use of minimally invasive analytical techniques, which revealed the presence of a waxy outer layer, tentatively identified as Japan wax, surrounding a Na-rich glass interior. The use of Japan wax in European glass production has never been ascertained so far.

MRS also permitted the identification of cadmium yellow and cadmium red, the colourizing agents responsible for the bright hues of bead types 10 and 12, respectively. Characteristic Raman bands found in the red glass of types 14 suggest that cuprite was used to produce this glass hue. Raman bands attributed to copper phosphates, sulfates and sulfides were also found in the type 48 bead, the pendant and the type 17 bead, respectively. Calcium phosphate, titanium dioxide, cassiterite and calcium antimonate were all identified by means of MRS.

In general, the opacifiers and colouring agent's time frame usage and application were found to be consistent with the proposed chronological and geographical origin of the beads.

### Acknowledgements

This work has been financially supported by a Concerted Research Action (GOA) of Ghent University and by Starting Grant No. 284126 of the European Research Council awarded to Koen Bostoen and by the Special Research Fund of Ghent University. The financial support of the FCT (Fundação para a Ciência e Tecnologia) project UID/Multi/04449/2013 and the COMPETE 2020 project POCI-01-0145-FEDER-007649 funded by the European Union is also acknowledged.

## References

[1] B. Clist, E. Cranshof, G.-M. de Schryver, D. Herremans, K. Karklins, I. Matonda, F. Steyaert, K. Bostoen, *Int. J. Hist. Archaeol.* **2015**, *19*, 464.
[2] B. Clist, E. Cranshof, G.-M. de Schryver, D. Herremans, K. Karklins, I. Matonda, C. Polet, A. Sengeløv, F. Steyaert, C. Verhaeghe, K. Bostoen, *African Archaeol. Rev.* **2015**, *32*, 369.
[3] C. Verhaeghe, B. Clist, C. Fontaine, K. Karklins, K. Bostoen, W. De Clercq, *BEADS J. Soc. Bead Res.* **2014**, *34*, 23.
[4] G. M. de Schryver, R. Grollemund, *Africana Linguist.* **2015**, *21*, 87.
[5] K. Bostoen, G. De Schryver, *Diachronica* **2015**, *2*, 284.
[6] A. Rousaki, A. Coccato, C. Verhaeghe, B. Clist, K. Bostoen, P. Vandenabeele, L. Moens, *Appl. Phys. A* **2016**, *70*, 79.
[7] J. Thornton, *Int. J. Afr. Hist. Stud.* **2001**, *34*, 89.
[8] C. Fromont, *The Art of Conversion: Christian Visual Culture in the Kingdom of Kongo*, The University of North Carolina Press, **2014**.
[9] J. K. Thornton, J. Vansina, G. Balandier, W. G. L. Randles, *J. Afr. Hist.* **2013**, *54*, 53.
[10] I. Kenyon, R. G. V. Hancock, S. Aufretier, *Archaeometry* **1995**, 37–323.
[11] R. G. V. Hancock, *Modern Methods for Analysing Archaeological and Historical Glass*, **2013**, p. 459.

[12] P. Robertshaw, M. Wood, A. Haour, K. Karklins, H. Neff, *J. Archaeol. Sci.* **2014**, *41*, 591.
[13] K. E. Kidd, M. A. Kidd, *BEADS J. Soc. Bead Res.* **2012**.
[14] K. Karklins, *Glass Beads: The Levin Catalogue of Mid-19th Century Beads: A Sample Book of 19th Century Venetian beads: Guide to the Description and Classification of Glass Beads*, Parcs Canada, Ottawa, **1985**.
[15] C. R. DeCorse, F. G. Richard, I. Thiaw, *J. African Archaeol.* **2003**, *1*, 77.
[16] R. H. Brill, *Chemical Analyses of Early Glasses* **1999**, *1*.
[17] L. Dussubieux, C. M. Kusimba, V. Gogte, S. B. Kusimba, B. Gratuze, R. Oka, *Archaeometry* **2008**, *50*, 797.
[18] P. Robertshaw, M. Wood, E. Melchiorre, R. S. Popelka-Filcoff, M. D. Glascock, *J. Archaeol. Sci.* **2010**, *37*, 1898.
[19] A. Tournié, L. C. Prinsloo, P. Colomban, *J. Raman Spectrosc.* **2012**, *43*, 532.
[20] M. Wood, S. Panighello, E. F. Orsega, P. Robertshaw, J. T. van Elteren, A. Crowther, M. Horton, N. Boivin, *Archaeol. Anthropol. Sci.* **2016**.
[21] L. C. Prinsloo, J. C. A. Boeyens, M. M. van der Ryst, G. Webb, *J. Mol. Struct.* **2012**, *1023*, 123.
[22] P. Robertshaw, B. Rasoarifetra, M. Wood, E. Melchiorre, R. S. Popelka-filcoff, M. D. Glascock, *J. African Archaeol.* **2006**, *4*, 91.
[23] K. Karklins, *BEADS J. Soc. Bead Res.* **1992**, *4*, 49.
[24] L. A. Ross, *Beads J. Soc. Bead Res.* **1990**, *2*, 29.
[25] A. Cesaratto, P. Sichel, D. Bersani, P. P. Lottici, A. Montenero, E. Salvioli-Mariani, M. Catarsi, *J. Raman Spectrosc.* **1682**, *2010*, 12.
[26] L. Robinet, C. Coupry, K. Eremin, C. Hall, *J. Raman Spectrosc.* **2006**, *37*, 789.
[27] L. Robinet, A. Bouquillon, J. Hartwig, *J. Raman Spectrosc.* **2008**, *39*, 618.
[28] P. Colomban, *Appl. Phys. A Mater. Sci. Process.* **2004**, *79*, 167.
[29] P. McMillan, *Am. Mineral.* **1984**, *69*, 622.
[30] B. O. Mysen, D. Virgo, C. M. Scarfe, *Am. Mineral.* **1980**, *65*, 690.
[31] S. Brawer, W. White, *J. Chem. Phys.* **1975**, *63*, 2421.
[32] P. Ricciardi, P. Colomban, A. Tournié, M. Macchiarola, N. Ayed, *J. Archaeol. Sci.* **2009**, *36*, 2551.
[33] P. Colomban, in *Raman Spectroscopy in Archaeology and Art History* (Eds: H. G. M. Edwards, J. M. Chalmers), **2005**, pp. 192–206.
[34] P. Colomban, A. Tournie, L. Bellot-Gurlet, *J. Raman Spectrosc.* **2006**, *37*, 841.
[35] B. Vekemans, K. Janssens, L. Vincze, F. Adams, P. Van Espen, *X-Ray Spectrom.* **1994**, *23*, 278.
[36] B. Vekemans, K. Janssens, L. Vincze, *Spectrochim. Acta – Part B* **1995**, *50*, 149.
[37] R. B. Scott, A. J. Shortland, P. Degryse, M. Power, K. Domoney, S. Boyen, D. Braekmans, *Glass Technol.* **2012**, *53*, 65.
[38] A. Bonneau, J.-F. Moreau, R. G. V. Hancock, K. Karklins, *BEADS J. Soc. Bead Res.* **2014**, *26*, 35.
[39] M. Regert, *Organic Mass Spectrometry in Art and Archaeology*, **2009**, pp. 97–129.
[40] M. Regert, J. Langlois, S. Colinart, *J. Chromatogr. A* **2005**, *1091*, 124.
[41] A. Asperger, W. Engewald, G. Fabian, *J. Anal. Appl. Pyrolysis* **1999**, *50*, 103.
[42] P. Mirti, P. Davit, M. Gulmini, *Anal. Bioanal. Chem.* **2002**, *372*, 221.
[43] A. J. Shortland, *Archaeometry* **2002**, *44*, 517.
[44] D. Möncke, M. Papageorgiou, A. Winterstein-Beckmann, N. Zacharias, *J. Archaeol. Sci.* **2014**, *46*, 23.
[45] A. Lima, T. Medici, A. Pires, D. Matos, M. Verità, *J. Archaeol. Sci.* **2012**, *39*, 1238.
[46] G. V. Rao, *Encycl. Sep. Sci. Acad. Press. New York* **2000**, *3491*.
[47] E. Marcoux, Y. Moëlo, J. M. Leistel, *Miner. Depos.* **1996**, *31*, 1.
[48] M. Frezzotti, F. Tecce, A. Casagli, *J. Geochemical Explor.* **2012**, *112*, 1.
[49] H. G. M. Edwards, E. M. Newton, J. Russ, *J. Mol. Struct.* **2000**, *551*, 245.
[50] M. A. Cortés-Jácome, G. Ferrat-Torres, L. F. F. Ortiz, C. Angeles-Chávez, E. López-Salinas, J. Escobar, M. L. Mosqueira, J. A. Toledo-Antonio, *Catal. Today* **2007**, *126*, 248.
[51] T. Ohsaka, S. Yamaoka, *Solid State Commun.* **1979**, *30*, 345.
[52] G. Penel, G. Leroy, C. Rey, E. Bres, *Calcif. Tissue Int.* **1998**, *63*, 475.
[53] J. G. Shapter, M. H. Brooker, W. M. Skinner, *Int. J. Miner. Process.* **2000**, *60*, 199.
[54] R. L. Frost, P. A. Williams, W. Martens, J. T. Kloprogge, and P. Leverett, **2002**, *33*, 260.
[55] T. P. Mernagh, A. G. Trudu, *Chem. Geol.* **1993**, *103*, 113.
[56] J. Krüger, P. Wlinkler, E. Lüderitz, M. Lück, H. U. Wolf, *Ullmann's Encycl. Ind. Chem.* **2012**, *6*, 113.
[57] S. Choi, S. Youm, *Can. Mineral.* **2000**, *38*, 567.
[58] R. Frost, P. Williams, W. Martens, *Am. Mineral.* **2004**, *89*, 1130.
[59] S. G. Tumanov, É. A. Filippova, *Glas. Ceram. (English Transl. Steklo i Keramika)* **1968**, 37.
[60] E. Cordoncillo, F. del Río, J. Carda, M. Llusar, P. Escribano, *J. Eur. Ceram. Soc.* **1998**, *18*, 1115.
[61] R. Eppler, *Ullmann's Encyclopedia of Industrial Chemistry*, **2000**, pp. 521–533.
[62] M. A. Tena, S. Meseguer, C. Gargori, A. Forés, J. A. Badenes, G. Monrós, *J. Eur. Ceram. Soc.* **2007**, *27*, 215.
[63] E. López-Navarrete, A. R. González-Elipe, M. Ocaña, *Ceram. Int.* **2003**, *29*, 385.
[64] P. Colomban, G. Sagon, X. Faurel, *J. Raman Spectrosc.* **2001**, *32*, 351.
[65] E. López-Navarrete, M. Ocaña, *J. Eur. Ceram. Soc.* **2002**, *22*, 353.
[66] B. Julián, H. Beltrán, E. Cordoncillo, P. Escribano, J. V. Folgado, M. Vallet-Regí, R. P. del Real, *Eur. J. Inorg. Chem.* **2002**, 2694.
[67] F. Rosi, C. Grazia, F. Gabrieli, A. Romani, M. Paolantoni, R. Vivani, B. G. Brunetti, P. Colomban, C. Miliani, *Microchem. J.* **2016**, *124*, 856.
[68] T. T. K. Chi, G. Gouadec, P. Colomban, G. Wang, L. Mazerolles, N. Q. Liem, *J. Raman Spectrosc.* **2011**, *42*, 1007.
[69] B. Tell, T. C. Damen, S. P. S. Porto, *Phys. Rev.* **1966**, *144*, 771.
[70] D. Xi, J. Li, Q. Pei, B. Chen, *Scan. Electron Microsc.* **2006**, *21*, 2911.
[71] A. M. Correia, R. J. H. Clark, M. I. M. Ribeiro, M. L. T. S. Duarte, *J. Raman Spectrosc* **2007**, *38*, 1390.
[72] H. G. M. Edwards, *Spectrochim. Acta – Part A Mol. Biomol. Spectrosc.* **2011**, *80*, 14.
[73] R. Feller, *Artist's pigments: A Handbook of Their History and Characteristics*, vol. *1*, National Gallery of Art and Archetype Publications Ltd., **1986**.
[74] C. W. Zhu, H. J. Wen, Y. X. Zhang, H. F. Fan, S. H. Fu, J. Xu, T. R. Qin, *Sci. China Earth Sci.* **2013**, *2056*, 12.
[75] H. Wen, C. Zhu, Y. Zhang, C. Cloquet, H. Fan, S. Fu, *Sci. Rep.* **2016**, *6*, 1.
[76] G. Van Der Snickt, J. Dik, M. Cotte, K. Janssens, J. Jaroszewicz, W. De Nolf, J. Groenewegen, L. Van Der Loeff, *Anal. Chem.* **2009**, *81*, 2600.
[77] M. Thoury, J. K. Delaney, E. R. de la Rie, M. Palmer, K. Morales, J. Krueger, *Appl. Spectrosc.* **2011**, *65*, 939.
[78] H. Norsker, J. Danisch, *Glazes – For the Self-reliant Potter*, Deutsches Zentrum fiir Entwicklungstechnologien – GATE, **1991**.
[79] M. Bouchard, *Spectrochim. Acta Part A Mol. Biomol. Spectrosc.* **2007**, *68*, 1101.
[80] G. Artioli, I. Angelini, *Modern Methods for Analysing Archaeological and Historical Glass*, **2013**, pp. 355–368.
[81] S. Cagno, P. Cosyns, K. Nys, K. Janssens, *Modern Methods for Analysing Archaeological and Historical Glass*, **2013**, pp. 369–385.
[82] N. Welter, U. Schüssler, W. Kiefer, *J. Raman Spectrosc.* **2007**, *38*, 113.
[83] L. C. Prinsloo, P. Colomban, *J. Raman Spectrosc.* **2008**, *39*, 79.
[84] C. MacRae, N. Wilson, *Microsc. Microanal.* **2008**, *14*, 184.
[85] A. Coccato, D. Bersani, A. Coudray, J. Sanyova, L. Moens, P. Vandenabeele, *J. Raman Spectrosc.* **2016**.
[86] H. J. Rosen, R. M. Macfarlane, E. M. Engler, V. Y. Lee, R. D. Jacowitz, *Phys. Rev. B* **1988**, *38*, 2460–2465.
[87] E. P. Bertin, *Principles and Practice of X-Ray Spectrometric Analysis*, 2nd ed., Plenum Press, **1978**.
[88] V. Gedzevičiūtė, N. Welter, U. Schüssler, C. Weiss, *Archaeol. Anthropol. Sci.* **2009**, *1*, 15.
[89] H. X. Zhao, Q. H. Li, S. Liu, F. X. Gan, *J. Raman Spectrosc.* **2013**, *44*, 643.
[90] H. G. M. Edwards, S. E. Jorge, J. Jehlicka, T. Munshi, *Spectrochim. Acta Part A* **2005**, *61*, 2273.
[91] M. Bouchard, D. C. Smith, *Spectrochim. Acta Part A Mol. Biomol. Spectrosc.* **2003**, *59*, 2247.
[92] R. B. Mason, M. S. Tite, *Archaeometry* **1997**, *39*, 41.
[93] Y. A. Guloyan, *Glas. Ceram. (English Transl. Steklo i Keramika)* **2015**, *71*, 303.

## Supporting information

Additional Supporting Information may be found online in the supporting information tab for this article.